

Flavour violating bosonic squark decays at LHC

A. Bartl¹, H. Eberl², E. Ginina¹, B. Herrmann³, K. Hidaka⁴,
W. Majerotto² and W. Porod⁵

¹ *Universität Wien, Fakultät für Physik, A-1090 Vienna, Austria*

² *Institut für Hochenergiephysik der Österreichischen Akademie der Wissenschaften, A-1050 Vienna, Austria*

³ *LAPTh, Université de Savoie, CNRS, 9 Chemin de Bellevue, B.P. 110, F-74941 Annecy-le-Vieux, France*

⁴ *Department of Physics, Tokyo Gakugei University, Koganei, Tokyo 184-8501, Japan*

⁵ *Institut für Theoretische Physik und Astrophysik, Universität Würzburg, D-97074 Würzburg, Germany*

Abstract

We study quark flavour violation (QFV) in the squark sector of the Minimal Supersymmetric Standard Model (MSSM). We assume mixing between the second and the third squark generations, i.e. $\tilde{c}_R - \tilde{t}_{L,R}$ mixing. We focus on QFV effects in bosonic squark decays, in particular on the decay into the lightest Higgs boson h^0 , $\tilde{u}_2 \rightarrow \tilde{u}_1 h^0$, where $\tilde{u}_{1,2}$ are the lightest up-type squarks. We show that the branching ratio of this QFV decay can be quite large (up to 50 %) due to large QFV trilinear couplings, and large $\tilde{c}_R - \tilde{t}_{L,R}$ and $\tilde{t}_L - \tilde{t}_R$ mixing, despite the strong constraints on QFV from B meson data. This can result in characteristic QFV final states with significant rates at LHC (14 TeV), such as $pp \rightarrow \tilde{g}\tilde{g}X \rightarrow t + h^0 + 3 \text{ jets} + \cancel{E}_T + X$ and $pp \rightarrow \tilde{g}\tilde{g}X \rightarrow tt \text{ (or } \bar{t}t) + h^0 + 2 \text{ jets} + \cancel{E}_T + X$. The QFV bosonic squark decays can have an influence on the squark and gluino searches at LHC.

1 Introduction

In most searches for supersymmetric (SUSY) particles at the LHC, the analyses have been performed within simplified SUSY models. However, SUSY extensions of the Standard Model (SM) can have a richer structure. In principle, mixing between the different squark generations is possible in the Minimal Supersymmetric Standard Model (MSSM). This can lead to quark flavour violating (QFV) effects, in addition to those induced by the Cabibbo-Kobayashi-Maskawa (CKM) matrix [1–3]. The mixing structure of the squark sector may be completely uncorrelated to the CKM matrix. Therefore, a detailed study of the consequences of general squark mixing is highly appropriate. Mixing between the 1st and the 2nd squark generations is strongly suppressed by K physics data [4]. Therefore, in this paper we assume mixing between the 2nd and the 3rd squark generations, respecting the constraints from B physics. Although these constraints are quite severe, they allow nevertheless substantial QFV effects.

In the MSSM, the mixing of the 2nd and the 3rd squark generations was theoretically studied for squark and gluino production and their decays at the LHC in the context of Minimal Flavour Violation (MFV) [5–7] as well as for general flavour mixing [8–16]. As shown in these papers the effects of QFV can be large. For example, in the case of mixing between scalar top and scalar charm, we can expect a large branching ratio (up to 40 %) of the QFV decay of the gluino, $\tilde{g} \rightarrow c\bar{t}(\bar{c}t)\tilde{\chi}_1^0$ [13]. This is due to the fact that the lightest up-squark mass eigenstates $\tilde{u}_{1,2}$ are mainly mixtures of \tilde{t}_R and \tilde{c}_R . Hence, \tilde{u}_1 and \tilde{u}_2 can both decay into $c\tilde{\chi}_1^0$ and $t\tilde{\chi}_1^0$.

In addition to the fermionic decays of squarks there are bosonic decays, $\tilde{q}_i \rightarrow \tilde{q}_j + Z^0, h^0, H^0, A^0$ and $\tilde{q}_i \rightarrow \tilde{q}'_j + W^\pm, H^\pm$, if kinematically allowed. In the quark flavour conserving (QFC) case, the most interesting decays are $\tilde{t}_2 \rightarrow \tilde{t}_1 + Z^0, h^0, H^0, A^0$; $\tilde{b}_2 \rightarrow \tilde{b}_1 + Z^0, h^0, H^0, A^0$; $\tilde{b}_2 \rightarrow \tilde{t}_1 + W^-, H^-$ [17, 18]. The QFV bosonic decays were recently considered in [11]. There the characteristic differences to the MFV case were worked out. A non-minimal flavour structure in the squark sector can change the entire squark decay pattern quite drastically, because many more transitions are possible.

In the present paper, we study the bosonic decays of the up-type squarks, $\tilde{u}_2 \rightarrow \tilde{u}_1 h^0/Z^0$, $\tilde{u}_3 \rightarrow \tilde{u}_{1,2} h^0/Z^0$, in the MSSM. Motivated by the recently observed signal of a Higgs boson at LHC, we are particularly interested in the bosonic QFV squark decays into the lightest Higgs boson, $\tilde{u}_2 \rightarrow \tilde{u}_1 h^0$. These decays offer the best possibility of determining the trilinear couplings $\tilde{q}_i - \tilde{q}_j - h^0$ entering the soft-SUSY-breaking Lagrangian. Another possibility would be to study the 3-body production $pp \rightarrow \tilde{q}_i \tilde{q}_j h^0$ as discussed for example in [19] for the QFC case. As the Higgs boson couples dominantly to the $\tilde{q}_L - \tilde{q}_R$ combination, one gets information from the decays $\tilde{q}_i \rightarrow \tilde{q}_j + h^0$ on the flavour structure of the left-right (LR) terms in the squark mass matrix. We study the mixing between the 2nd and the 3rd generation of up-type squarks, i.e. $\tilde{c}_R - \tilde{t}_{L,R}$ mixing. There are strong constraints on this mixing from B physics (see also [20]), Higgs boson searches and SUSY particle searches (see Appendix B). We take into account all these constraints in our analysis.

The paper is organized as follows: In Section 2 we shortly give the definitions of the QFV squark mixing parameters. In Section 3 we discuss the QFV bosonic decays of

up-type squarks in detail in a definite scenario accesible at LHC. We also consider two further scenarios, one GUT inspired and another one, where the bosonic decays of \tilde{u}_2 dominate over the fermionic decays. Section 4 contains a discussion of various QFV final states to be expected at LHC with $\sqrt{s} = 14$ TeV. In Section 5 we give a summary. In the Appendices we show explicitly the part of the interaction Lagrangian which is most relevant for this study and summarize the experimental and theoretical constraints on the MSSM parameters, especially those on the QFV parameters, mainly from B physics.

2 Squark mixing with flavour violation

In the MSSM the most general form of the squark mass matrices in the super-CKM basis of $\tilde{q}_{0\gamma} = (\tilde{q}_{1L}, \tilde{q}_{2L}, \tilde{q}_{3L}, \tilde{q}_{1R}, \tilde{q}_{2R}, \tilde{q}_{3R})$, $\gamma = 1, \dots, 6$, with $(q_1, q_2, q_3) = (u, c, t)$, (d, s, b) is [21]

$$\mathcal{M}_{\tilde{q}}^2 = \begin{pmatrix} \mathcal{M}_{\tilde{q},LL}^2 & \mathcal{M}_{\tilde{q},LR}^2 \\ \mathcal{M}_{\tilde{q},RL}^2 & \mathcal{M}_{\tilde{q},RR}^2 \end{pmatrix}, \quad (1)$$

for $\tilde{q} = \tilde{u}, \tilde{d}$, where the 3×3 matrices read

$$\begin{aligned} \mathcal{M}_{\tilde{u},LL}^2 &= V_{\text{CKM}} M_Q^2 V_{\text{CKM}}^\dagger + D_{\tilde{u},LL} \mathbf{1} + \hat{m}_u^2, \\ \mathcal{M}_{\tilde{u},RR}^2 &= M_U^2 + D_{\tilde{u},RR} \mathbf{1} + \hat{m}_u^2, \\ \mathcal{M}_{\tilde{d},LL}^2 &= M_Q^2 + D_{\tilde{d},LL} \mathbf{1} + \hat{m}_d^2, \\ \mathcal{M}_{\tilde{d},RR}^2 &= M_D^2 + D_{\tilde{d},RR} \mathbf{1} + \hat{m}_d^2. \end{aligned} \quad (2)$$

Here $M_{Q,U,D}$ are the hermitian soft SUSY-breaking mass matrices of the squarks and $\hat{m}_{u,d}$ are the diagonal mass matrices of the up-type and down-type quarks. $D_{\tilde{q},LL} = \cos 2\beta m_Z^2 (T_3^q - e_q \sin^2 \theta_W)$ and $D_{\tilde{q},RR} = e_q \sin^2 \theta_W \times \cos 2\beta m_Z^2$, where T_3^q and e_q are the isospin and electric charge of the quarks (squarks), respectively, and θ_W is the weak mixing angle. The left-left blocks of up-type and down-type squarks are related by the CKM matrix V_{CKM} due to the $SU(2)_L$ symmetry. The off-diagonal blocks of eq. (1) read

$$\begin{aligned} \mathcal{M}_{\tilde{u},RL}^2 = \mathcal{M}_{\tilde{u},LR}^{2\dagger} &= \frac{v_2}{\sqrt{2}} T_U^T - \mu^* \hat{m}_u \cot \beta, \\ \mathcal{M}_{\tilde{d},RL}^2 = \mathcal{M}_{\tilde{d},LR}^{2\dagger} &= \frac{v_1}{\sqrt{2}} T_D^T - \mu^* \hat{m}_d \tan \beta, \end{aligned} \quad (3)$$

where $T_{U,D}^T$ are the transposes of the soft SUSY-breaking trilinear coupling matrices of the up-type and down-type squarks $T_{U,D}$ defined as $\mathcal{L}_{\text{int}} \supset -(T_{U\alpha\beta} \tilde{u}_{R\beta}^\dagger \tilde{u}_{L\alpha} H_2^0 + T_{D\alpha\beta} \tilde{d}_{R\beta}^\dagger \tilde{d}_{L\alpha} H_1^0)$, μ is the higgsino mass parameter, and $\tan \beta = v_2/v_1$, where $v_{1,2} = \sqrt{2} \langle H_{1,2}^0 \rangle$ are the vacuum expectation values of the neutral Higgs fields. The squark mass matrices are diagonalized by the 6×6 unitary matrices $R^{\tilde{q}}$, $\tilde{q} = \tilde{u}, \tilde{d}$, such that

$$R^{\tilde{q}} \mathcal{M}_{\tilde{q}}^2 (R^{\tilde{q}})^\dagger = \text{diag}(m_{\tilde{q}_1}^2, \dots, m_{\tilde{q}_6}^2) \quad (4)$$

with $m_{\tilde{q}_1} < \dots < m_{\tilde{q}_6}$. The physical mass eigenstates $\tilde{q}_i, i = 1, \dots, 6$ are given by $\tilde{q}_i = R_{i\alpha}^{\tilde{q}} \tilde{q}_{0\alpha}$.

We define the QFV parameters in the up-type squark sector $\delta_{\alpha\beta}^{LL}$, $\delta_{\alpha\beta}^{uRR}$ and $\delta_{\alpha\beta}^{uRL}$ ($\alpha \neq \beta$) as follows [22]:

$$\delta_{\alpha\beta}^{LL} \equiv M_{Q\alpha\beta}^2 / \sqrt{M_{Q\alpha\alpha}^2 M_{Q\beta\beta}^2}, \quad (5)$$

$$\delta_{\alpha\beta}^{uRR} \equiv M_{U\alpha\beta}^2 / \sqrt{M_{U\alpha\alpha}^2 M_{U\beta\beta}^2}, \quad (6)$$

$$\delta_{\alpha\beta}^{uRL} \equiv (v_2/\sqrt{2})T_{U\beta\alpha} / \sqrt{M_{U\alpha\alpha}^2 M_{Q\beta\beta}^2}. \quad (7)$$

Here $\alpha, \beta = 1, 2, 3$ ($\alpha \neq \beta$) denote the quark flavours u, c, t . The QFV parameters relevant for this study are δ_{23}^{uRL} , $\delta_{23}^{uLR} \equiv (\delta_{32}^{uRL})^*$, δ_{23}^{uRR} , and δ_{23}^{LL} , which are the $\tilde{c}_R - \tilde{t}_L$, $\tilde{c}_L - \tilde{t}_R$, $\tilde{c}_R - \tilde{t}_R$, and $\tilde{c}_L - \tilde{t}_L$ mixing parameters, respectively. We also use the QFC parameter δ_{33}^{uRL} which is defined by eq. (7) with $\alpha = \beta = 3$ and is the $\tilde{t}_L - \tilde{t}_R$ mixing parameter. We assume all QFV parameters and δ_{33}^{uRL} to be real.

3 QFV bosonic decays of up-type squarks

If kinematically allowed, the following QFV bosonic decays of up-type squarks are possible:

$$\tilde{u}_i \rightarrow \tilde{u}_j + h^0, H^0, A^0 \quad (8)$$

$$\tilde{u}_i \rightarrow \tilde{d}_j + H^+ \quad (9)$$

$$\tilde{u}_i \rightarrow \tilde{u}_j + Z^0 \quad (10)$$

$$\tilde{u}_i \rightarrow \tilde{d}_j + W^+ \quad (11)$$

with $i, j = 1, \dots, 6$ specifying the squark mass eigenstates which are mixtures of the squark flavour eigenstates (see Section 2). Here h^0 (H^0) is the lighter (heavier) CP-even neutral Higgs boson, A^0 is the CP-odd neutral Higgs boson, and H^+ is the charged Higgs boson. Of course, there are also QFC bosonic squark decays. In this article we study mainly \tilde{u}_2 decays in scenarios where their decays into charged bosons of eqs. (9) and (11) and those into the heavier Higgs bosons H^0 and A^0 are kinematically forbidden. The couplings between $\tilde{u}_i - \tilde{u}_j/\tilde{d}_j$ and the bosons in eqs. (8) – (11), taking into account QFV, are given in [11]. For completeness, the couplings to the lightest Higgs boson, h^0 , are listed in Appendix A. Note that the QFV parts are proportional to the soft-SUSY-breaking trilinear coupling parameter T_U . In the following discussion of the decays we adopt the QFV parameters δ_{23}^{LL} , δ_{23}^{uRR} , δ_{23}^{uRL} , δ_{23}^{uLR} as defined in Section 2. The parameters δ_{23}^{uLR} , δ_{23}^{uRL} are proportional to T_{U23} and T_{U32} , respectively. In case $\tilde{u}_{1,2}$ are strong mixtures of $\tilde{c}_R - \tilde{t}_R - \tilde{t}_L$, a measurement of the branching ratio of the decay $\tilde{u}_2 \rightarrow \tilde{u}_1 h^0$ gives important information on the QFV trilinear coupling T_{U32} (i.e. $\tilde{c}_R^\dagger - \tilde{t}_L - H_2^0$ coupling).

In the calculation of the branching ratios of the decays (8) – (11) we have to take into

account both QFV and QFC fermionic squark decays [10, 13]

$$\tilde{u}_i \rightarrow u_\alpha + \tilde{\chi}_k^0 \quad (12)$$

$$\tilde{u}_i \rightarrow d_\alpha + \tilde{\chi}_l^+ \quad (13)$$

$$\tilde{u}_i \rightarrow u_\alpha + \tilde{g} \quad (14)$$

where $\alpha = 1, 2, 3$ is the flavour index, $\tilde{\chi}_k^0, k = 1, \dots, 4$, are the neutralinos and $\tilde{\chi}_l^+, l = 1, 2$, are the charginos. As $\tilde{u}_{1,2}$ are mainly mixtures of \tilde{c}_R, \tilde{t}_R and \tilde{t}_L in the scenarios under consideration, both decays $\tilde{u}_{1,2} \rightarrow t\tilde{\chi}_1^0$ and $\tilde{u}_{1,2} \rightarrow c\tilde{\chi}_1^0$ are possible.

Table 1: Weak scale basic MSSM parameters at $Q = 1$ TeV [23] for scenario A, except for m_{A^0} which is the pole mass (i.e. the physical mass) of A^0 . All of $T_{U\alpha\alpha}$ and $T_{D\alpha\alpha}$ are zero, except for $T_{U33} = -2160$ GeV (i.e. $\delta_{33}^{uRL} = -0.34$). All other squark parameters not shown here are zero.

M_1	M_2	M_3
400 GeV	800 GeV	1000 GeV

μ	$\tan \beta$	m_{A^0}
2640 GeV	20	1500 GeV

	$\alpha = 1$	$\alpha = 2$	$\alpha = 3$
$M_{Q\alpha\alpha}^2$	$(2400)^2 \text{ GeV}^2$	$(2360)^2 \text{ GeV}^2$	$(1450)^2 \text{ GeV}^2$
$M_{U\alpha\alpha}^2$	$(2380)^2 \text{ GeV}^2$	$(780)^2 \text{ GeV}^2$	$(750)^2 \text{ GeV}^2$
$M_{D\alpha\alpha}^2$	$(2380)^2 \text{ GeV}^2$	$(2340)^2 \text{ GeV}^2$	$(2300)^2 \text{ GeV}^2$

δ_{23}^{LL}	δ_{23}^{uRR}	δ_{23}^{uRL}	δ_{23}^{uLR}
0	0.3	-0.07	0

In the following we first study the QFV bosonic decays in detail for the scenario with the parameters in Table 1 (scenario A). In a second step we consider two variants of this scenario which contain substantial new features. The parameters are chosen such that the two lightest u -squarks and the gluino can be produced with sizable rates at the LHC with $\sqrt{s} = 14$ TeV. Moreover, the mass difference between \tilde{u}_2 and \tilde{u}_1 is such that the decay $\tilde{u}_2 \rightarrow \tilde{u}_1 h^0$ is kinematically possible. We choose relatively large values of M_1, M_2 and μ in order to avoid the dominance of the fermionic squark decays of \tilde{u}_2 . The hierarchy between the values of $M_{Q\alpha\alpha}^2$ and $M_{U\alpha\alpha}^2, \alpha = 1, 2, 3$, is chosen to allow sizable $\tilde{c}_R - \tilde{t}_L$ mixing effects. For this scenario all experimental and theoretical constraints given in Appendix B are satisfied. In particular, $m_{\tilde{g}}, m_{\tilde{q}}$ (for the first and the second generation) and $m_{\tilde{\chi}_1^0}$ obey the experimental bounds. For the low-energy observables we obtain the following values: $\Delta M_{B_s} = 16.4 \text{ ps}^{-1}$, $\text{B}(b \rightarrow s\gamma) = 3.0 \cdot 10^{-4}$, $\text{B}(B_s \rightarrow \mu^+\mu^-) = 3.3 \cdot 10^{-9}$. All numerical

Table 2: Physical masses in GeV of the particles in scenario A (see Table 1).

$m_{\tilde{\chi}_1^0}$	$m_{\tilde{\chi}_2^0}$	$m_{\tilde{\chi}_3^0}$	$m_{\tilde{\chi}_4^0}$	$m_{\tilde{\chi}_1^+}$	$m_{\tilde{\chi}_2^+}$
397	824	2623	2625	825	2625

m_{h^0}	m_{H^0}	m_{A^0}	m_{H^\pm}
124.0	1496	1500	1510

$m_{\tilde{g}}$	$m_{\tilde{u}_1}$	$m_{\tilde{u}_2}$	$m_{\tilde{u}_3}$	$m_{\tilde{u}_4}$	$m_{\tilde{u}_5}$	$m_{\tilde{u}_6}$
1141	605	861	1477	2387	2401	2427

$m_{\tilde{d}_1}$	$m_{\tilde{d}_2}$	$m_{\tilde{d}_3}$	$m_{\tilde{d}_4}$	$m_{\tilde{d}_5}$	$m_{\tilde{d}_6}$
1433	2321	2364	2388	2404	2428

Table 3: Flavour decomposition of \tilde{u}_1 and \tilde{u}_2 in scenario A of Table 1. Shown are the squared coefficients.

	\tilde{u}_L	\tilde{c}_L	\tilde{t}_L	\tilde{u}_R	\tilde{c}_R	\tilde{t}_R
\tilde{u}_1	0	0	0.032	0	0.209	0.759
\tilde{u}_2	0	0	0.031	0	0.785	0.184

Table 4: Two-body decay branching ratios of \tilde{u}_2 , \tilde{u}_1 and gluino in scenario A of Table 1. The charge conjugated processes have the same branching ratios and are not shown explicitly.

$B(\tilde{u}_2 \rightarrow \tilde{u}_1 h^0)$	0.47
$B(\tilde{u}_2 \rightarrow \tilde{u}_1 Z^0)$	0.01
$B(\tilde{u}_2 \rightarrow c \tilde{\chi}_1^0)$	0.43
$B(\tilde{u}_2 \rightarrow t \tilde{\chi}_1^0)$	0.09
$B(\tilde{u}_1 \rightarrow c \tilde{\chi}_1^0)$	0.36
$B(\tilde{u}_1 \rightarrow t \tilde{\chi}_1^0)$	0.64
$B(\tilde{g} \rightarrow \tilde{u}_2 \bar{c})$	0.12
$B(\tilde{g} \rightarrow \tilde{u}_2 \bar{t})$	0.01
$B(\tilde{g} \rightarrow \tilde{u}_1 \bar{c})$	0.09
$B(\tilde{g} \rightarrow \tilde{u}_1 \bar{t})$	0.27

calculations in this study, except for the cross sections, are performed with the public code

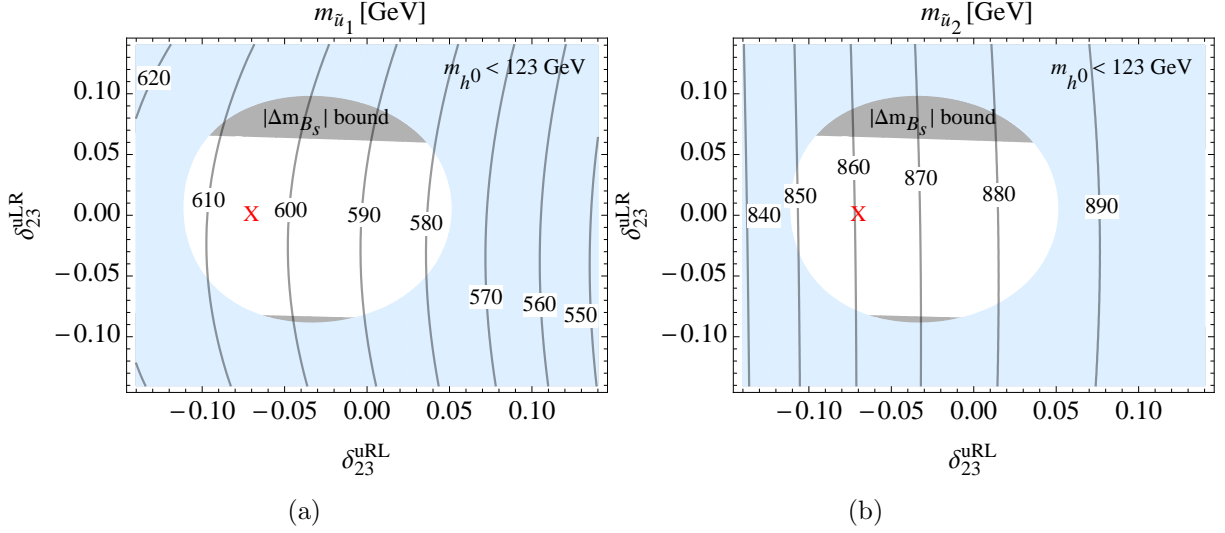


Figure 1: Dependence of the masses of \tilde{u}_1 (a) and \tilde{u}_2 (b) on δ_{23}^{uRL} and δ_{23}^{uLR} where the other parameters are fixed as in Table 1 and "X" in both plots corresponds to scenario A.

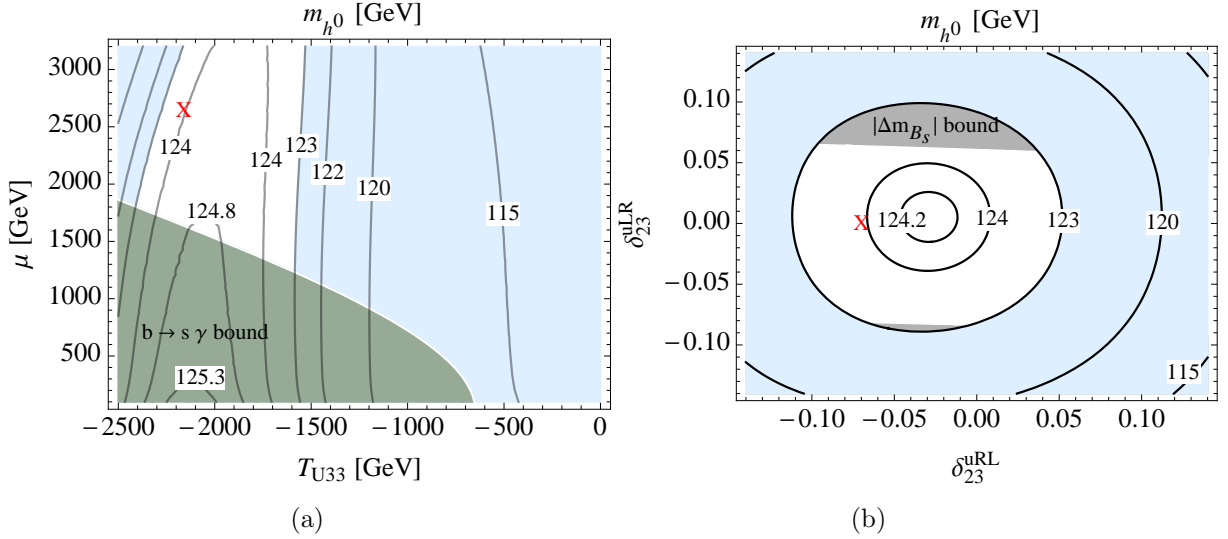


Figure 2: The mass of the lightest Higgs boson, m_{h^0} , as a function of T_{U33} and μ (a) and as a function of δ_{23}^{uRL} and δ_{23}^{uLR} (b) where the other parameters are fixed as in Table 1 and "X" in both plots corresponds to scenario A. The light shaded (light blue) areas indicate $m_{h^0} < 123$ GeV (see Table 10).

SPheno v3.2 [24, 25]. We also use the package SSP [26] that allows an efficient handling of parameter studies. The physical masses of squarks, gluino, charginos, neutralinos and Higgs bosons are shown in Table 2. We obtain $m_{h^0} = 124$ GeV which is in the range of the Higgs signal at LHC [27–29]. Moreover, in this scenario we are in the decoupling limit

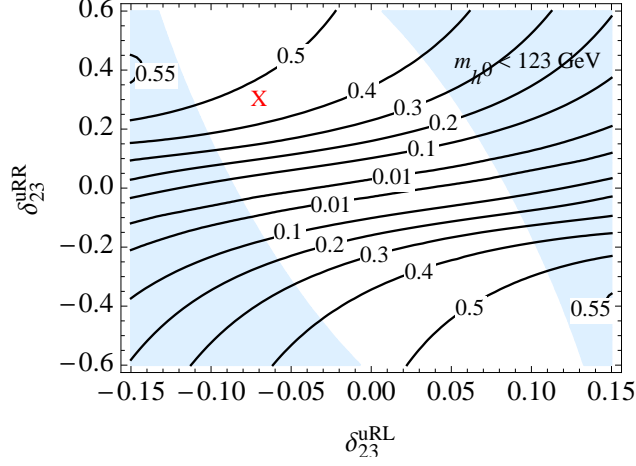


Figure 3: The branching ratio $B(\tilde{u}_2 \rightarrow \tilde{u}_1 h^0)$ as a function of δ_{23}^{uRL} and δ_{23}^{uRR} in scenario A. "X" indicates the reference point defined with the parameters of Table 1.

with $m_{A^0} = 1500 \text{ GeV} \gg m_{h^0}$, and hence the lightest Higgs boson h^0 is SM-like. The flavour decompositions of \tilde{u}_1 and \tilde{u}_2 in scenario A are shown in Table 3. In this scenario with large δ_{23}^{uRR} , δ_{33}^{uRL} and δ_{23}^{uRL} , \tilde{u}_1 is mainly a $\tilde{t}_R - \tilde{c}_R(-\tilde{t}_L)$ mixture and \tilde{u}_2 is mainly a $\tilde{c}_R - \tilde{t}_R(-\tilde{t}_L)$ mixture.

We studied the QFV fermionic decays of gluinos and squarks in [10, 13, 14]. There it turned out that QFV effects mainly depend on δ_{23}^{uRR} and δ_{23}^{dRR} , whereas the influence of the other QFV parameters is much weaker. In Table 1 we have taken $\delta_{23}^{uRR} = 0.3$ in order to have the branching ratios for the QFV decays $\tilde{u}_1 \rightarrow c\tilde{\chi}_1^0$ and $\tilde{u}_1 \rightarrow t\tilde{\chi}_1^0$ comparable. In the present paper we concentrate on the dependence of the QFV effects on δ_{23}^{uRL} and δ_{23}^{uLR} , which enter the squark-squark-Higgs couplings.

In Fig. 1(a) and 1(b) we show the mass contours of \tilde{u}_1 and \tilde{u}_2 in the $\delta_{23}^{uRL} - \delta_{23}^{uLR}$ plane for scenario A with all other parameters as in Table 1. In all contour plots in this article the white regions satisfy all the experimental and theoretical constraints listed in B. One can see a somewhat stronger dependence on δ_{23}^{uRL} due to the sizable mass-splitting induced by the $\tilde{c}_R - \tilde{t}_L$ mixing, which is a consequence of the chosen hierarchy within M_Q^2 and M_U^2 .

In Fig. 2(a) the lightest Higgs mass m_{h^0} is shown as a function of T_{U33} and μ . In order to obtain m_{h^0} within the allowed parameter range a large $|T_{U33}|$ and a rather large μ [30–32] are required. A large $|T_{U33}|$ enhances the stop loop corrections and a large $|\mu|$ enlarges the sbottom loop corrections through the term $A_b - \mu \tan \beta$. In Fig. 2(b) we show contours of m_{h^0} in the $\delta_{23}^{uLR} - \delta_{23}^{uRL}$ plane. Within the shown range of the QFV parameters, m_{h^0} varies by about 1.5 GeV due to the \tilde{c} admixture in the stop loops.

Next we study the decay $\tilde{u}_2 \rightarrow \tilde{u}_1 h^0$ in more detail. In Fig. 3 we show the branching ratio $B(\tilde{u}_2 \rightarrow \tilde{u}_1 h^0)$ as a function of δ_{23}^{uRL} and δ_{23}^{uRR} . Note that δ_{23}^{uRR} must be different from 0 in order to have this branching ratio sizable. At the reference point of scenario A (see Table 1) $B(\tilde{u}_2 \rightarrow \tilde{u}_1 h^0) \approx 0.45$. The δ_{23}^{uRL} and δ_{23}^{uRR} dependences can be understood by the arguments below. Note that $\tilde{u}_{1,2}$ become strong mixtures of \tilde{c}_R and \tilde{t}_R for sizable

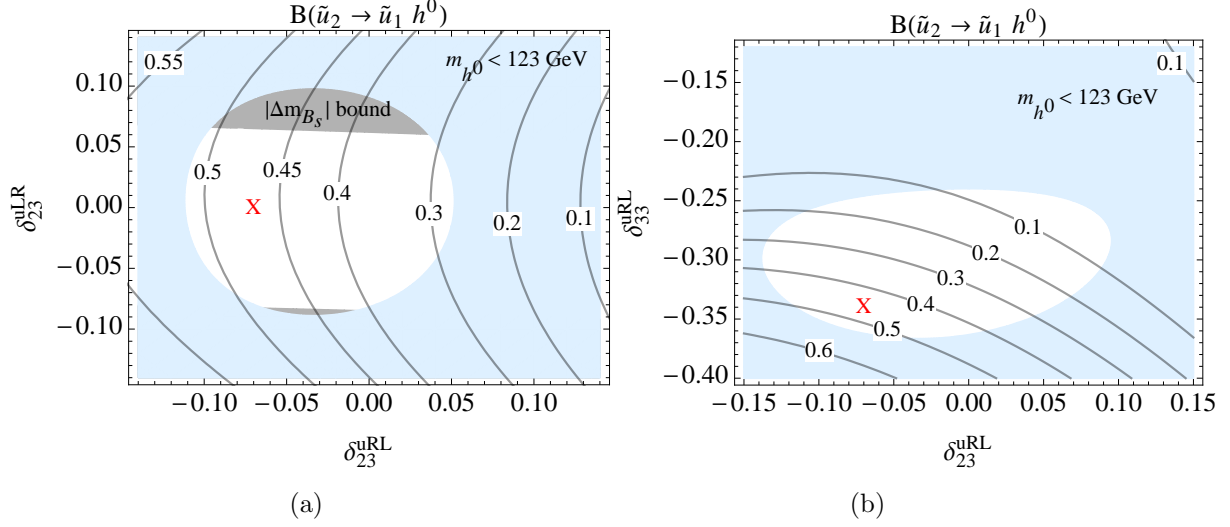


Figure 4: The branching ratio of the decay $\tilde{u}_2 \rightarrow \tilde{u}_1 h^0$ as a function of δ_{23}^{uRL} and δ_{23}^{uLR} (a) and as a function of δ_{23}^{uRL} and δ_{33}^{uRL} (b) with the other parameters fixed as in Table 1 and "X" in both plots corresponds to scenario A.

δ_{23}^{uRR} .

In Fig. 4(a) we show the branching ratio of the decay $\tilde{u}_2 \rightarrow \tilde{u}_1 h^0$ as a function of the QFV parameters δ_{23}^{uRL} and δ_{23}^{uLR} . We have used the formulas eqs. (26), (27) and (28) of Appendix A. The dominant terms in the coupling $c_{\tilde{u}_2 \tilde{u}_1 h^0}$ are those proportional to T_{U33} and T_{U32} , since $\tilde{u}_{1,2}$ are mainly mixtures of \tilde{c}_R, \tilde{t}_R and \tilde{t}_L (recall that $\delta_{23}^{uRL} \sim T_{U32}$, $\delta_{23}^{uLR} \sim T_{U23}$, $\delta_{33}^{uRL} \sim T_{U33}$, see eq. (7)). The term proportional to T_{U23} is rather small due to the small \tilde{c}_L components of $\tilde{u}_{1,2}$. Therefore, the dependence on δ_{23}^{uRL} is stronger than that on δ_{23}^{uLR} . In the region allowed by the constraints listed in Appendix B the branching ratio for $\tilde{u}_2 \rightarrow \tilde{u}_1 h^0$ can go up to 50%. The decrease of $B(\tilde{u}_2 \rightarrow \tilde{u}_1 h^0)$ with increasing δ_{23}^{uRL} is due to an interference of the dominant terms with the couplings T_{U33} and T_{U32} in eq. (27).

In Fig. 4(b) we show the branching ratio $B(\tilde{u}_2 \rightarrow \tilde{u}_1 h^0)$ as a function of the QFV parameter δ_{23}^{uRL} and the QFC parameter δ_{33}^{uRL} (recall that δ_{33}^{uRL} corresponds to the $\tilde{t}_L - \tilde{t}_R$ mixing). The decrease of $B(\tilde{u}_2 \rightarrow \tilde{u}_1 h^0)$ with increasing δ_{23}^{uRL} is due to the same reason as in Fig. 4(a). $B(\tilde{u}_2 \rightarrow \tilde{u}_1 h^0)$ grows with increasing $|\delta_{33}^{uRL}|$ because T_{U33} as well as the \tilde{t}_L components of $\tilde{u}_{1,2}$ become larger.

In Table 4 we give the branching ratios for the two-body decays of \tilde{u}_2, \tilde{u}_1 and gluino at the reference point of scenario A. Note that the $\tilde{c}_R - \tilde{t}_R$ mixing and the $\tilde{c}_R - \tilde{t}_L$ mixing together with the large top trilinear coupling T_{U33} lead to an enhanced branching ratio for $\tilde{u}_2 \rightarrow \tilde{u}_1 h^0$.

We have also studied the QFV decays $\tilde{u}_3 \rightarrow \tilde{u}_1 h^0$ and $\tilde{u}_3 \rightarrow \tilde{u}_2 h^0$. The branching ratio of $\tilde{u}_3 \rightarrow \tilde{u}_1 h^0$ can go up to 30%. At the reference point of Table 1 it is about 23%. \tilde{u}_3 has a large \tilde{t}_L component. Hence, the decay $\tilde{u}_3 \rightarrow \tilde{u}_1 h^0$ is mainly due to $\tilde{t}_L \rightarrow \tilde{t}_R h^0$ transitions. On the other hand, in the decay $\tilde{u}_3 \rightarrow \tilde{u}_2 h^0$ the behaviour of the branching ratio is very different, because the $\tilde{t}_L - \tilde{c}_R$ transitions are more important. Its branching ratio at the

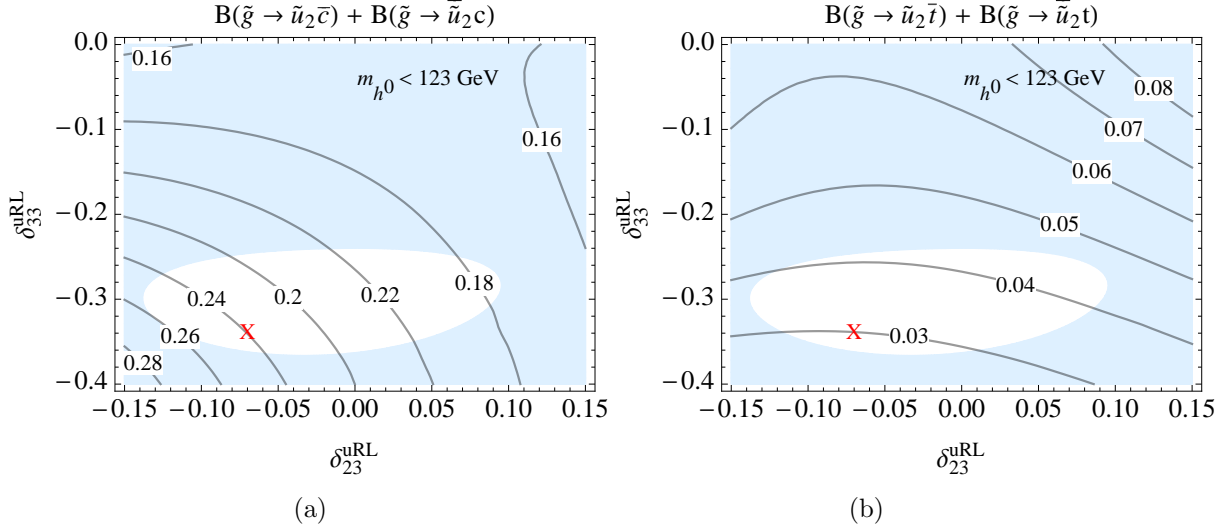


Figure 5: The branching ratios $B(\tilde{g} \rightarrow \tilde{u}_2 \bar{c}) + B(\tilde{g} \rightarrow \tilde{u}_2 c)$ (a) and $B(\tilde{g} \rightarrow \tilde{u}_2 \bar{t}) + B(\tilde{g} \rightarrow \tilde{u}_2 t)$ (b) as functions of δ_{23}^{uRL} and δ_{33}^{uRL} with the other parameters fixed as in Table 1 and "X" in both plots corresponds to scenario A.

reference point is about 10%. The branching ratios of $\tilde{u}_3 \rightarrow \tilde{u}_1 Z^0$ and $\tilde{u}_3 \rightarrow \tilde{u}_2 Z^0$ at the reference point are about 28% and 13%, respectively.

In scenario A the squark \tilde{u}_2 can also be produced in the decay of the gluino. We show in Fig. 5(a) and 5(b) the branching ratios of the decays $\tilde{g} \rightarrow \tilde{u}_2 \bar{c} + c.c.$ and $\tilde{g} \rightarrow \tilde{u}_2 \bar{t} + c.c.$ as functions of δ_{23}^{uRL} and δ_{33}^{uRL} . The branching ratio of the decay $\tilde{g} \rightarrow \tilde{u}_2 \bar{t} + c.c.$ is much smaller than that of $\tilde{g} \rightarrow \tilde{u}_2 \bar{c} + c.c.$ due to phase space and because the \tilde{c}_R component of \tilde{u}_2 is larger than the $\tilde{t}_{L,R}$ components. In Table 4 we give all of the branching ratios of gluino decays (except charge conjugate decays) for the reference point of scenario A.

Note that in this scenario the gaugino mass parameters M_1 , M_2 , and M_3 do not obey the GUT relation $M_1 \approx 0.5 M_2$, $M_3/M_2 = g_3^2/g_2^2$, where g_2 and g_3 are the SU(2) and SU(3) gauge coupling constants, respectively. We define a variant of scenario A by replacing in Table 1 only the gaugino mass parameters by

$$M_1 = 250 \text{ GeV}, \quad M_2 = 500 \text{ GeV}, \quad M_3 = 1500 \text{ GeV} \quad (15)$$

which satisfy approximately the GUT relations. We call it scenario B. The physical masses of the squarks are almost the same as in Table 2 and we do not show them explicitly. In this scenario the gluino is relatively heavy, $m_{\tilde{g}} = 1626 \text{ GeV}$, therefore, it has a relatively small pair production cross section $pp \rightarrow \tilde{g}\tilde{g}X$ (3.5 fb). As we will see in the next section, gluino production is important, because the lighter squarks $\tilde{u}_{1,2}$ are also produced in the gluino decays $\tilde{g} \rightarrow \tilde{u}_{1,2} \bar{q}$. In this scenario the dependences of m_h^0 and $B(\tilde{u}_2 \rightarrow \tilde{u}_1 h^0)$ on the QFV and QFC parameters are very similar to those of scenario A, shown in Figs. 2 and 4. The two-body decay branching ratios of \tilde{u}_2 , \tilde{u}_1 and gluino for scenario B are shown in Table 5.

Table 5: Two-body decay branching ratios of \tilde{u}_2 , \tilde{u}_1 and gluino in scenario B, see Table 1 and eq. (15). The charge conjugated processes have the same branching ratios and are not shown explicitly.

$B(\tilde{u}_2 \rightarrow \tilde{u}_1 h^0)$	0.39
$B(\tilde{u}_2 \rightarrow \tilde{u}_1 Z^0)$	0.01
$B(\tilde{u}_2 \rightarrow c\tilde{\chi}_1^0)$	0.45
$B(\tilde{u}_2 \rightarrow t\tilde{\chi}_1^0)$	0.10
$B(\tilde{u}_1 \rightarrow c\tilde{\chi}_1^0)$	0.26
$B(\tilde{u}_1 \rightarrow t\tilde{\chi}_1^0)$	0.73
$B(\tilde{g} \rightarrow \tilde{u}_2 \bar{c})$	0.16
$B(\tilde{g} \rightarrow \tilde{u}_2 t)$	0.04
$B(\tilde{g} \rightarrow \tilde{u}_1 \bar{c})$	0.07
$B(\tilde{g} \rightarrow \tilde{u}_1 t)$	0.22

Table 6: Physical masses in GeV of the particles in scenario C, see Table 1 and eq. (16).

$m_{\tilde{\chi}_1^0}$	$m_{\tilde{\chi}_2^0}$	$m_{\tilde{\chi}_3^0}$	$m_{\tilde{\chi}_4^0}$	$m_{\tilde{\chi}_1^+}$	$m_{\tilde{\chi}_2^+}$
398	819	2623	2625	819	2625

m_{h^0}	m_{H^0}	m_{A^0}	m_{H^\pm}
123.7	1497	1500	1537

$m_{\tilde{g}}$	$m_{\tilde{u}_1}$	$m_{\tilde{u}_2}$	$m_{\tilde{u}_3}$	$m_{\tilde{u}_4}$	$m_{\tilde{u}_5}$	$m_{\tilde{u}_6}$
1134	651	800	1580	2387	2401	2427

$m_{\tilde{d}_1}$	$m_{\tilde{d}_2}$	$m_{\tilde{d}_3}$	$m_{\tilde{d}_4}$	$m_{\tilde{d}_5}$	$m_{\tilde{d}_6}$
807	2321	2363	2388	2404	2428

Table 7: Flavour decomposition of \tilde{u}_1 and \tilde{u}_2 in scenario C, see Table 1 and eq. (16). Shown are the squared coefficients.

	\tilde{u}_L	\tilde{c}_L	\tilde{t}_L	\tilde{u}_R	\tilde{c}_R	\tilde{t}_R
\tilde{u}_1	0	0	0.242	0	0.745	0.012
\tilde{u}_2	0	0	0.713	0	0.255	0.032

In scenarios A and B the decay $\tilde{u}_2 \rightarrow \tilde{u}_1 Z^0$ has a very small branching ratio. In the

following we present a scenario (scenario C) where the branching ratios of $\tilde{u}_2 \rightarrow \tilde{u}_1 h^0$ and $\tilde{u}_2 \rightarrow \tilde{u}_1 Z^0$ are both large. For this purpose we have again changed some of the MSSM parameters with respect to Table 1, leaving all other parameters unchanged,

$$M_{U22}^2 = (650 \text{ GeV})^2, \quad M_{U33}^2 = (1600 \text{ GeV})^2, \quad M_{Q33}^2 = (780 \text{ GeV})^2, \\ \delta_{23}^{uRR} = 0, \quad \delta_{23}^{uRL} = -0.17, \quad \delta_{33}^{uRL} = -0.3. \quad (16)$$

Table 8: Two-body decay branching ratios of \tilde{u}_2 , \tilde{u}_1 and gluino in scenario C, see Table 1 and eq. (16). The charge conjugated processes have the same branching ratios and are not shown explicitly.

$B(\tilde{u}_2 \rightarrow \tilde{u}_1 h^0)$	0.43
$B(\tilde{u}_2 \rightarrow \tilde{u}_1 Z^0)$	0.34
$B(\tilde{u}_2 \rightarrow c \tilde{\chi}_1^0)$	0.17
$B(\tilde{u}_2 \rightarrow t \tilde{\chi}_1^0)$	0.06
$B(\tilde{u}_1 \rightarrow c \tilde{\chi}_1^0)$	0.96
$B(\tilde{u}_1 \rightarrow t \tilde{\chi}_1^0)$	0.04
$B(\tilde{g} \rightarrow \tilde{u}_2 \bar{c})$	0.04
$B(\tilde{g} \rightarrow \tilde{u}_2 \bar{t})$	0.08
$B(\tilde{g} \rightarrow \tilde{u}_1 \bar{c})$	0.19
$B(\tilde{g} \rightarrow \tilde{u}_1 \bar{t})$	0.05

In particular, the QFV trilinear coupling parameter $\delta_{23}^{uRL} (\sim T_{U32})$ is much larger than in scenario A. This new scenario satisfies all experimental and theoretical constraints listed in Appendix B. The physical masses, the flavour decomposition of \tilde{u}_1 and \tilde{u}_2 as well as the branching ratios of the two-body decays of the squarks and gluino in scenario C are shown in Table 6, Table 7 and Table 8, respectively. As both $B(\tilde{u}_2 \rightarrow \tilde{u}_1 h^0)$ and $B(\tilde{u}_2 \rightarrow \tilde{u}_1 Z^0)$ are very large, this leads to the dominance of the QFV bosonic decays of \tilde{u}_2 . Note also that $\tilde{u}_{1,2}$ are mixtures of \tilde{c}_R and \tilde{t}_L due to the sizable QFV trilinear coupling $T_{U32} \sim \delta_{23}^{uRL}$, which significantly enhances the QFV decay $\tilde{u}_2 \rightarrow \tilde{u}_1 h^0$. The large $B(\tilde{u}_2 \rightarrow \tilde{u}_1 Z^0)$ is mainly due to the sizable \tilde{t}_L component in $\tilde{u}_{1,2}$ in this scenario, whereas in scenarios A and B the \tilde{t}_L component is small. In Fig. 6 we show $B(\tilde{u}_2 \rightarrow \tilde{u}_1 Z^0)$ and $B(\tilde{u}_2 \rightarrow \tilde{u}_1 h^0)$ as functions of δ_{23}^{uRL} . We see that the ratio $B(\tilde{u}_2 \rightarrow \tilde{u}_1 Z^0)/B(\tilde{u}_2 \rightarrow \tilde{u}_1 h^0)$ is sensitive to the QFV as well as to the QFC SUSY parameters. These results do not change for $\delta_{23}^{uRL} \rightarrow -\delta_{23}^{uRL}$.

4 Characteristic final states

In this section we discuss some characteristic final states to be expected at LHC, $\sqrt{s} = 14 \text{ TeV}$, from the QFV decays of \tilde{u}_2 into the lightest Higgs boson h^0 within the scenarios

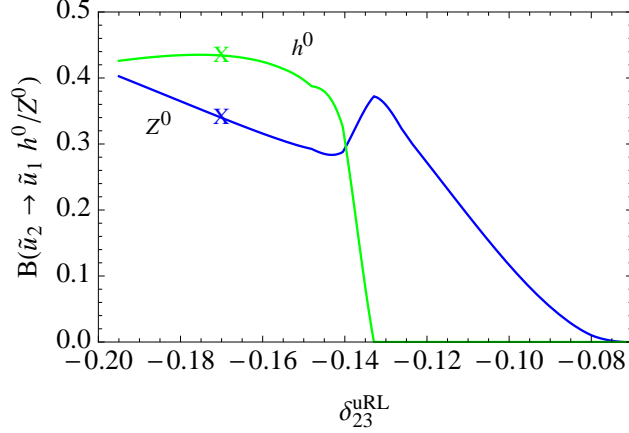


Figure 6: δ_{23}^{uRL} dependence of the branching ratios $B(\tilde{u}_2 \rightarrow \tilde{u}_1 h^0)$ and $B(\tilde{u}_2 \rightarrow \tilde{u}_1 Z^0)$ in scenario C. "X" indicates the reference point defined with the parameters of Table 1, except for those shown in eq. (16). The vanishing of $B(\tilde{u}_2 \rightarrow \tilde{u}_1 h^0)$ at $\delta_{23}^{uRL} \approx -0.13$ is due to kinematics, which also causes the peak of $B(\tilde{u}_2 \rightarrow \tilde{u}_1 Z^0)$.

considered. The lighter squark states can be produced directly, $pp \rightarrow \tilde{u}_1 \tilde{u}_1 X$, $pp \rightarrow \tilde{u}_2 \tilde{u}_2 X$, or via gluino production, $pp \rightarrow \tilde{g} \tilde{g} X$, where at least one of the gluinos decays into \tilde{u}_1 or \tilde{u}_2 , $\tilde{g} \rightarrow \tilde{u}_{1,2} c; \tilde{u}_{1,2} t$. The $\tilde{u}_{1,2}$ and gluino decays relevant for our study are as follows:

$$\tilde{u}_1 \rightarrow c/t \tilde{\chi}_1^0, \quad (17)$$

$$\tilde{u}_2 \rightarrow c/t \tilde{\chi}_1^0, \quad (18)$$

$$\tilde{u}_2 \rightarrow \tilde{u}_1 h^0/Z^0 \rightarrow c/t \tilde{\chi}_1^0 h^0/Z^0, \quad (19)$$

$$\tilde{g} \rightarrow \tilde{u}_1 \bar{c}/\bar{t} \rightarrow c/t \tilde{\chi}_1^0 \bar{c}/\bar{t} \text{ (and } c.c.), \quad (20)$$

$$\tilde{g} \rightarrow \tilde{u}_2 \bar{c}/\bar{t} \rightarrow c/t \tilde{\chi}_1^0 \bar{c}/\bar{t} \text{ (and } c.c.), \quad (21)$$

$$\tilde{g} \rightarrow \tilde{u}_2 \bar{c}/\bar{t} \rightarrow \tilde{u}_1 h^0/Z^0 \bar{c}/\bar{t} \rightarrow c/t \tilde{\chi}_1^0 h^0/Z^0 \bar{c}/\bar{t} \text{ (and } c.c.). \quad (22)$$

We assume that $\tilde{\chi}_1^0$ is the lightest supersymmetric particle (LSP) and gives rise to missing transverse energy \cancel{E}_T in experiment. The corresponding combined decay branching ratios are given, for example, by

$$B(\tilde{u}_2 \rightarrow c/t \tilde{\chi}_1^0 h^0/Z^0) = B(\tilde{u}_2 \rightarrow \tilde{u}_1 h^0/Z^0) B(\tilde{u}_1 \rightarrow c/t \tilde{\chi}_1^0), \quad (23)$$

$$B(\tilde{g} \rightarrow c/t \tilde{\chi}_1^0 \bar{c}/\bar{t}) = 2[B(\tilde{g} \rightarrow \tilde{u}_1 \bar{c}/\bar{t}) B(\tilde{u}_1 \rightarrow c/t \tilde{\chi}_1^0) + B(\tilde{g} \rightarrow \tilde{u}_2 \bar{c}/\bar{t}) B(\tilde{u}_2 \rightarrow c/t \tilde{\chi}_1^0)], \quad (24)$$

$$B(\tilde{g} \rightarrow c/t \tilde{\chi}_1^0 h^0/Z^0 \bar{c}/\bar{t}) = 2B(\tilde{g} \rightarrow \tilde{u}_2 \bar{c}/\bar{t}) \times B(\tilde{u}_2 \rightarrow \tilde{u}_1 h^0/Z^0) B(\tilde{u}_1 \rightarrow c/t \tilde{\chi}_1^0). \quad (25)$$

In Table 9 we list the processes leading to at least one Higgs boson h^0 in the final state in association with jets and top-quarks. We assume that the c -quarks hadronize to jets, similarly to u -quarks. Of course, additional c -tagging would be very helpful.

In Table 9, t denotes a top-quark or an anti-top-quark and j denotes a c/\bar{c} -quark jet. What concerns the final states from $\tilde{u}_2 \tilde{u}_2$ pair production, the final states with one t

Table 9: Possible final states containing at least one Higgs boson h^0 expected from the decays of \tilde{u}_2 into h^0 and Z^0 . t denotes top-quark or anti-top-quark; j denotes a c/\bar{c} -quark jet; \cancel{E}_T is missing transverse energy due to the two LSP neutralinos $\tilde{\chi}_1^0$ in the final state; X contains only the beam jets. Note that in general the states with h^0 replaced by Z^0 are also possible. We also give the corresponding cross sections in scenario A, in case they exceed 1 fb.

processes	final states containing h^0
$pp \rightarrow \tilde{u}_2 \tilde{u}_2 X$	$2j + h^0 + \cancel{E}_T + X$ (1.5 fb) $j + t + h^0 + \cancel{E}_T + X$ (2.8 fb) $2t + h^0 + \cancel{E}_T + X$ $2j + 2h^0 + \cancel{E}_T + X$ $j + t + 2h^0 + \cancel{E}_T + X$ (1 fb) $2t + 2h^0 + \cancel{E}_T + X$ $2j + h^0 + Z^0 + \cancel{E}_T + X$ $j + t + h^0 + Z^0 + \cancel{E}_T + X$ $2t + h^0 + Z^0 + \cancel{E}_T + X$

processes	final states containing h^0
$pp \rightarrow \tilde{g} \tilde{g} X$	$4j + h^0 + \cancel{E}_T + X$ (2 fb) $3j + t + h^0 + \cancel{E}_T + X$ (8 fb) $2j + 2t + h^0 + \cancel{E}_T + X$ (13 fb) $4j + 2h^0 + \cancel{E}_T + X$ $3j + t + 2h^0 + \cancel{E}_T + X$ $2j + 2t + 2h^0 + \cancel{E}_T + X$ $4j + h^0 + Z^0 + \cancel{E}_T + X$ $3j + t + h^0 + Z^0 + \cancel{E}_T + X$ $2j + 2t + h^0 + Z^0 + \cancel{E}_T + X$

are explicitly QFV whereas those with no t and $2t$ look like QFC. The cross sections for $pp \rightarrow \tilde{u}_2 \tilde{u}_2 X$ and $pp \rightarrow \tilde{u}_2 \tilde{u}_2 X$ are smaller than 1 fb. Concerning the final states from gluino pair production, those with one t and $3t$ are explicitly QFV whereas those with no t and $4t$ look like QFC. Note that the final states with $3t$ and $4t$ are not shown in Table 9 since the corresponding cross sections are very small (much less than 1 fb). The states with $2t$ are explicitly QFV in case they are $t\bar{t}$ or $t\bar{t}$. On the other hand, they look like QFC in case they are $t\bar{t}$. The events with $t\bar{t}$ can stem from QFV and QFC gluino decays, e.g. $\tilde{g}\tilde{g} \rightarrow (c\bar{t}h^0\tilde{\chi}_1^0) + (t\bar{c}h^0\tilde{\chi}_1^0)$ and $\tilde{g}\tilde{g} \rightarrow (t\bar{t}h^0\tilde{\chi}_1^0) + (c\bar{c}h^0\tilde{\chi}_1^0)$. Note also that the events

with $t\bar{t}(\text{or } t\bar{t})jj$, such as $t\bar{t}(\text{or } t\bar{t})jjh^0\cancel{E}_T X$ (where X contains only the beam jets) can practically not be produced in the QFC MSSM (nor in the SM). The detection of such events could be useful for discriminating between the QFC MSSM and QFV MSSM.

For scenario A, the production cross section for $pp \rightarrow \tilde{g}\tilde{g}X$ is 148 fb including one-loop SUSY-QCD corrections. For calculating this cross section we have used Prospino 2 [33] as the cross section is only very weakly dependent on the QFV parameters. The cross sections for $pp \rightarrow \tilde{u}_2\tilde{u}_2X$, $pp \rightarrow \tilde{g}\tilde{u}_1X$, and $pp \rightarrow \tilde{g}\tilde{u}_2X$ are at tree-level 10 fb, 1 fb, and 1.4 fb, respectively. For the calculation of these cross sections we have used FeynArts and FormCalc [34, 35]. All numbers for the cross sections given in this section include the charge conjugate final states.

In scenario A (Table 1), using the decay branching ratios of \tilde{u}_2 and \tilde{u}_1 , as shown in Table 4, we find that the produced $\tilde{u}_2\tilde{u}_2$ state goes into the final state $2j + h^0 + \cancel{E}_T$ with a probability of 15%. Hence, in our scenario, the corresponding cross section for $pp \rightarrow \tilde{u}_2\tilde{u}_2X \rightarrow 2j + h^0 + \cancel{E}_T + X$ is about 1.5 fb. Note, however, that this final state can also occur in the QFC bosonic decays. On the other hand, the process $pp \rightarrow \tilde{u}_2\tilde{u}_2X \rightarrow j + t + h^0 + \cancel{E}_T + X$ is QFV and the corresponding cross section is almost 2.8 fb. Even the cross section for $pp \rightarrow \tilde{u}_2\tilde{u}_2X \rightarrow j + t + 2h^0 + \cancel{E}_T + X$ is about 1 fb. As the ratio $B(\tilde{u}_2 \rightarrow \tilde{u}_1 Z^0)/B(\tilde{u}_2 \rightarrow \tilde{u}_1 h^0)$ is only about 0.02 in scenario A, the probability for the $\tilde{u}_2\tilde{u}_2$ system to decay into the final state $2j + Z^0 + h^0 + \cancel{E}_T$ is only 0.1%.

The squarks \tilde{u}_2 are also produced in gluino decays. The branching ratios for the gluino decays at the reference point of scenario A are given in Table 4. For the process $\tilde{g}\tilde{g} \rightarrow \tilde{u}_2\tilde{u}_2jj \rightarrow 4j + h^0 + \cancel{E}_T + X$ one gets a probability of 0.8%, leading to a cross section for $pp \rightarrow \tilde{g}\tilde{g}X \rightarrow \tilde{u}_2\tilde{u}_2jjX \rightarrow 4j + h^0 + \cancel{E}_T + X$ of about 1.2 fb. (Here the contributions of $pp \rightarrow \tilde{g}\tilde{g}X \rightarrow \tilde{u}_2\tilde{u}_2jjX$ are also included.) In the process $pp \rightarrow \tilde{g}\tilde{g}X \rightarrow \tilde{u}_2\tilde{u}_2jjX$ the final state $4j + 2h^0 + \cancel{E}_T + X$ is possible with a probability of approximately 0.3%. The cross section for $pp \rightarrow \tilde{g}\tilde{g}X \rightarrow 4j + 2h^0 + \cancel{E}_T + X$ is 0.5 fb.

A further interesting process is $pp \rightarrow \tilde{g}\tilde{g}X \rightarrow \tilde{u}_1\tilde{u}_2jjX \rightarrow 4j + h^0 + \cancel{E}_T + X$, having a probability of 0.5%, giving a cross section of 0.8 fb. (We have included also $pp \rightarrow \tilde{g}\tilde{g}X \rightarrow \tilde{u}_1\tilde{u}_2$.) Therefore, one has a cross section of 2 fb altogether for $pp \rightarrow \tilde{g}\tilde{g}X \rightarrow 4j + h^0 + \cancel{E}_T + X$. The QFV final state $3j + t + h^0 + \cancel{E}_T + X$ coming from $pp \rightarrow \tilde{g}\tilde{g}X$ has a cross section of 8 fb. Correspondingly, the final state $2j + 2t + h^0 + \cancel{E}_T + X$ from $pp \rightarrow \tilde{g}\tilde{g}X$ has a cross section of 13 fb, containing a QFC contribution of 5 fb (see also Fig. 7(a)). The cross section of $pp \rightarrow \tilde{g}\tilde{g}X \rightarrow 3j + t + 2h^0 + \cancel{E}_T + X$ is almost 0.9 fb. In Table 9 we give the corresponding cross sections in case they exceed 1 fb.

Summing up the cross sections for all final states with at least one h^0 in scenario A one gets 28 fb, 16 fb of which come from pure QFV final states. This means that one could expect about 1600 of such events assuming an integrated luminosity of 100 fb^{-1} at LHC (14 TeV).

In Fig. 7(a) we show the cross sections for $pp \rightarrow \tilde{g}\tilde{g}X \rightarrow 3j + t + h^0 + \cancel{E}_T + X$ and $pp \rightarrow \tilde{g}\tilde{g}X \rightarrow 2j + 2t + h^0 + \cancel{E}_T + X$ in scenario A as a function of δ_{23}^{uRL} . The red solid line corresponds to the pure QFV final state $3j + t + h^0 + \cancel{E}_T + X$. The green solid line corresponds to the pure QFV final state $t\bar{t}/t\bar{t} + 2j + h^0 + \cancel{E}_T + X$ plus the final state $t\bar{t} + 2j + h^0 + \cancel{E}_T + X$ coming from the QFV gluino decays. Note that the number of the

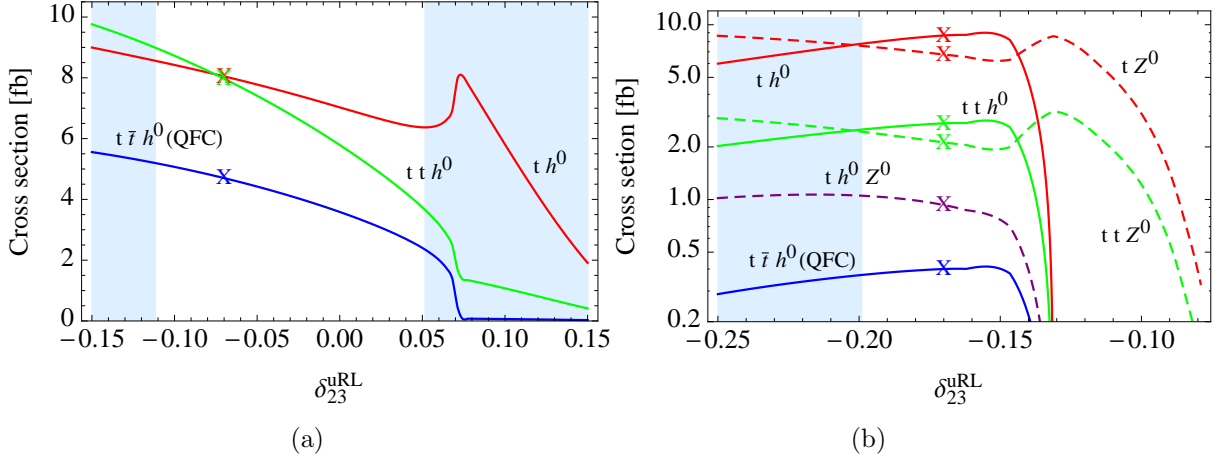


Figure 7: Cross sections for the final states coming from gluino pair production and subsequent decays $\tilde{g} \rightarrow \tilde{u}_{1,2} c/t$, $\tilde{u}_2 \rightarrow \tilde{u}_1 h^0/Z^0$ at LHC, $\sqrt{s} = 14$ TeV, (a) in scenario A and (b) in scenario C as functions of δ_{23}^{uRL} . The red solid (dashed) line corresponds to the pure QFV final state $3j + t + h^0$ (Z^0) + \cancel{E}_T + X. The green solid (dashed) line corresponds to the QFV events $tt/\bar{t}\bar{t}/t\bar{t} + 2j + h^0$ (Z^0) + \cancel{E}_T + X coming from the QFV gluino decays. The blue solid line corresponds to the events $t + \bar{t} + 2j + h^0$ + \cancel{E}_T + X coming from the QFC gluino decays. The violet dashed line corresponds to the pure QFV final state $3j + t + h^0 + Z^0$ + \cancel{E}_T + X. "X" indicates the corresponding scenario's reference point: for scenario A defined with the parameters of Table 1, and for scenario C defined with the parameters of Table 1, except for those shown in eq. (16). The shaded (light blue) areas are excluded by $m_h^0 < 123$ GeV.

$tt/\bar{t}\bar{t}$ final state events is exactly equal to the number of the $t\bar{t}$ final state events coming from the QFV gluino decays due to the Majorana nature of the gluino. The blue solid line corresponds to the QFC events $t + \bar{t} + 2j + h^0$ + \cancel{E}_T + X coming from the QFC gluino decays. For $\delta_{23}^{uRL} > 0.074$ the decay $\tilde{u}_1 \rightarrow t\tilde{\chi}_1^0$ is kinematically not possible whereas the decay $\tilde{u}_2 \rightarrow t\tilde{\chi}_1^0$ is still allowed (with 18% branching ratio). Note that the QFV cross sections do not vanish for $\delta_{23}^{uRL} = 0$ because the other QFV parameter δ_{23}^{uRR} is not zero.

In the GUT inspired scenario (scenario B) the gluino is much heavier and therefore the cross section $\sigma(pp \rightarrow \tilde{g}\tilde{g}X)$ is much smaller being 3.5 fb. The final state coming from $pp \rightarrow \tilde{u}_2\tilde{u}_2X$ have the same cross section as in scenario A, whereas the cross sections for the final states due to $pp \rightarrow \tilde{g}\tilde{g}X$ are about a factor of 40 smaller.

The third scenario (scenario C) is characterized by a higher branching ratio $B(\tilde{u}_2 \rightarrow \tilde{u}_1 Z^0) = 34\%$, see Table 8. Therefore, one expects final states with Z^0 and h^0 . As the gluino mass is very close to that of scenario A, the cross section for $pp \rightarrow \tilde{g}\tilde{g}X$ is 148 fb. Consequently, the cross section $\sigma(pp \rightarrow \tilde{g}\tilde{g}X \rightarrow 3j + t + h^0 + \cancel{E}_T + X)$ is 8.5 fb and $\sigma(pp \rightarrow \tilde{g}\tilde{g}X \rightarrow 3j + t + Z^0 + \cancel{E}_T + X)$ is 6.8 fb. In Fig. 7(b) we show the cross sections analogous to those shown in Fig. 7(a), but for scenario C. In addition, we also show the cross sections of the final states containing a Z^0 . The green dashed line corresponds to the pure QFV final state $tt/\bar{t}\bar{t} + 2j + Z^0 + \cancel{E}_T + X$ plus the final state $t\bar{t} + 2j + Z^0 + \cancel{E}_T + X$

coming from the QFV gluino decays. The number of the $t\bar{t}/t\bar{t}$ final state events is again equal to the number of the QFV $t\bar{t}$ final state events. The violet dashed line corresponds to the pure QFV final state $3j + t + h^0 + Z^0 + \cancel{E}_T + X$. Fig. 7(b) is symmetric for $\delta_{23}^{uRL} \rightarrow -\delta_{23}^{uRL}$.

We want to comment shortly on the background processes to the QFV bosonic squark decay signals containing at least one Higgs boson h^0 . An important background is the production of a Higgs boson h^0 in association with top quarks, $pp \rightarrow t\bar{t}h^0X$, where h^0 is radiated off from top or anti-top. The cross section at $\sqrt{s} = 14$ TeV is about 400 fb. In these events, however, there is no missing energy, \cancel{E}_T (apart from the missing energy coming from possible semi-leptonic decays of the top-quarks), therefore it should be possible to separate them from the signal. Further Higgs boson production processes are $pp \rightarrow Z^0Z^0h^0; W^+W^-h^0$. They will of course, constitute a background to the $h^0 + jets + \cancel{E}_T$. However, these processes do not contain a top in the final state. As discussed above, events with top (anti-top) in the final states together with a h^0 are the most significant ones for QFV. Single h^0 production from gluon-gluon fusion as well as $pp \rightarrow b\bar{b}h^0X$ do not contain a top quark in the final state either.

Concerning the background within the general MS SM, the situation can be more complex. In the scenarios considered the charginos and neutralinos are relatively heavy, so that the decays of the lightest squarks $\tilde{u}_{1,2}$ into these play a minor role, except those into the lightest neutralino. If this is not the case the QFV signals will be less pronounced.

The most interesting final states exhibiting QFV in bosonic squark decays are $j + t + h^0 + \cancel{E}_T + X$ from $\tilde{u}_2\tilde{u}_2$ production and $3j + t + h^0 + \cancel{E}_T + X$ from $\tilde{g}\tilde{g}$ production. To extract these events, the identification of the top-quark and the Higgs boson by their decay products would be crucial. This would require Monte Carlo studies including appropriate cuts and detector simulation. However, this is beyond the scope of this paper.

5 Summary

In this paper we have studied the effects of QFV in the bosonic squark decays $\tilde{u}_2 \rightarrow \tilde{u}_1h^0/Z^0$ at the LHC. We have assumed mixing between the second and third up-squark generations, that is $\tilde{c}_R - \tilde{t}_{L,R}$ mixing. In our calculations, we have taken into account all experimental constraints from B meson data on ΔM_{B_s} , $B(b \rightarrow s\gamma)$, $B(B_s \rightarrow \mu\mu)$, limits on the gluino and squark masses, the latest data on the lightest Higgs boson mass and the theoretical constraints on the trilinear couplings from the vacuum stability conditions. We have found that the branching ratio $B(\tilde{u}_2 \rightarrow \tilde{u}_1h^0)$ can be larger than in the QFC case, and can go up to 50%. The decay $\tilde{u}_2 \rightarrow \tilde{u}_1h^0$ can give access to the QFV trilinear couplings T_{U32} and T_{U23} . We have studied the characteristic final states expected from the QFV decay $\tilde{u}_2 \rightarrow \tilde{u}_1h^0$ at LHC with $\sqrt{s} = 14$ TeV in three different scenarios. We have considered direct \tilde{u}_2 production $pp \rightarrow \tilde{u}_2\tilde{u}_2X$ as well as \tilde{u}_2 production in \tilde{g} decays via $pp \rightarrow \tilde{g}\tilde{g}X$. In two scenarios (A and C) we have taken $m_{\tilde{g}} \approx 1100$ GeV and in the third scenario (B) $m_{\tilde{g}} \approx 1600$ GeV. The most pronounced QFV final state is $3j + t + h^0 + \cancel{E}_T + X$, coming from $pp \rightarrow \tilde{g}\tilde{g}X \rightarrow \tilde{u}_{1,2}\tilde{t}\tilde{u}_2\bar{c}X \rightarrow \tilde{u}_{1,2}\tilde{t}\tilde{u}_1h^0\bar{c}X \rightarrow c\bar{c}c\bar{c}h^0\cancel{E}_TX$, which can have a

Table 10: Constraints on the MSSM parameters from the B-physics experiments relevant mainly for the mixing between the second and the third generations of squarks and from the limit on the h^0 mass. The fourth column shows constraints at 95% CL obtained by combining the experimental error quadratically with the theoretical uncertainty, except for $B(B_s \rightarrow \mu\mu)$ and m_{h^0} . $R_{B \rightarrow \tau\nu}^{\text{SUSY}} \equiv \frac{B(B^+ \rightarrow \tau^+\nu)_{\text{SUSY}}}{B(B^+ \rightarrow \tau^+\nu)_{\text{SM}}} \approx [1 - ((m_{B^+} \tan \beta)/m_{H^+})^2]^2$ where m_{H^+} is the H^+ mass [37].

Observable	Exp. data	Theor. uncertainty	Constr. (95%CL)
ΔM_{B_s} [ps ⁻¹]	17.725 ± 0.049 (68% CL) [38]	± 3.3 (95% CL) [39]	17.73 ± 3.30
$10^4 \times B(b \rightarrow s\gamma)$	3.37 ± 0.23 (68% CL) [40]	± 0.23 (68% CL) [41]	3.37 ± 0.64
$10^6 \times B(b \rightarrow s l^+ l^-)$ ($l = e$ or μ)	1.60 ± 0.50 (68% CL) [42]	± 0.11 (68% CL) [43]	1.60 ± 1.00
$10^9 \times B(B_s \rightarrow \mu^+ \mu^-)$	< 4.2 (95% CL) [44]		$1.1 < 10^9 \times B < 4.2$
$10^4 \times B(B^+ \rightarrow \tau^+ \nu)$	$1.1 < 10^9 \times B < 6.4$ (95% CL) [45] 1.15 ± 0.23 (68% CL) [46]	± 0.25 (68% CL) [47]	$R_{B \rightarrow \tau\nu}^{\text{SUSY}} =$ 0.96 ± 0.54
m_{h^0} [GeV]	125.3 ± 0.64 (68% CL)(CMS), 126.0 (ATLAS) [27–29]	± 2 [36]	$123 < m_{h^0} < 129$

cross section up to 8 fb in scenario A. For extracting these events, an identification of the top quark and the Higgs boson would be required.

In conclusion, our analysis suggests that for a complete determination of the parameters of the squark mass matrices in the MSSM it would be necessary to study both the fermionic and the bosonic QFC and QFV decays of squarks. This can also have an influence on the squark and gluino searches at LHC.

Acknowledgments

This work is supported by the "Fonds zur Förderung der wissenschaftlichen Forschung (FWF)" of Austria, project No. I 297-N16, by the DFG, project No. PO-1337/2-1 and by DAAD, project PROCOPE 54366394.

A Up-squark decays into h^0

In the super-CKM basis, the Lagrangian including the coupling of up-type squarks to the lighter neutral Higgs boson, h^0 , is given by

$$\begin{aligned} \mathcal{L} = & -\frac{g_2}{2m_W} h^0 \left[\tilde{u}_{iL}^* \tilde{u}_{jL} \left(m_W^2 \sin(\alpha + \beta) \left(1 - \frac{1}{3} \tan^2 \theta_W \right) \delta_{ij} + 2 \frac{\cos \alpha}{\sin \beta} m_{u,i}^2 \delta_{ij} \right) \right. \\ & + \tilde{u}_{iR}^* \tilde{u}_{jR} \left(m_W^2 \sin(\alpha + \beta) \frac{4}{3} \tan^2 \theta_W \delta_{ij} + 2 \frac{\cos \alpha}{\sin \beta} m_{u,i}^2 \delta_{ij} \right) \\ & \left. + \left[\tilde{u}_{iR}^* \tilde{u}_{jL} \left(\mu^* \frac{\sin \alpha}{\sin \beta} m_{u,i} \delta_{ij} + \frac{\cos \alpha}{\sin \beta} \frac{v_2}{\sqrt{2}} (T_U)_{ji} \right) + \text{h.c.} \right] \right], \end{aligned} \quad (26)$$

where α is the mixing angle of the two CP-even Higgs bosons, h^0 and H^0 . The terms proportional to m_W^2 stem from the D-terms of the scalar potential and the expressions with quark masses $m_{u,d}$ stem from Yukawa and F-terms. They are all flavour-universal. The trilinear couplings are explicit breaking terms that couple left-handed to right-handed squarks. Inserting the transformations to the physical fields, $\tilde{u}_{iL} = (R^{\tilde{u}\dagger})_{ik} \tilde{u}_k$ and $\tilde{u}_{iR} = (R^{\tilde{u}\dagger})_{(i+3)k} \tilde{u}_k$, eq. (26) can be written in terms of physical up-type squark fields as $\mathcal{L} = c_{\tilde{u}_i \tilde{u}_j h^0} \tilde{u}_j^* \tilde{u}_i h^0$ with the coupling

$$\begin{aligned} c_{\tilde{u}_i \tilde{u}_j h^0} = & -\frac{g_2}{2m_W} \left[m_W^2 \sin(\alpha + \beta) \left[\left(1 - \frac{1}{3} \tan^2 \theta_W \right) \right. \right. \\ & \times (R^{\tilde{u}})_{jk} (R^{\tilde{u}\dagger})_{ki} + \frac{4}{3} \tan^2 \theta_W (R^{\tilde{u}})_{j(k+3)} (R^{\tilde{u}\dagger})_{(k+3)i} \Big] \\ & + 2 \frac{\cos \alpha}{\sin \beta} \left[(R^{\tilde{u}})_{jk} m_{u,k}^2 (R^{\tilde{u}\dagger})_{ki} + (R^{\tilde{u}})_{j(k+3)} m_{u,k}^2 (R^{\tilde{u}\dagger})_{(k+3)i} \right] \\ & + \frac{\sin \alpha}{\sin \beta} \left[\mu^* (R^{\tilde{u}})_{j(k+3)} m_{u,k} (R^{\tilde{u}\dagger})_{ki} + \mu (R^{\tilde{u}})_{jk} m_{u,k} (R^{\tilde{u}\dagger})_{(k+3)i} \right] \\ & \left. + \frac{\cos \alpha}{\sin \beta} \frac{v_2}{\sqrt{2}} \left[(R^{\tilde{u}})_{j(k+3)} (T_U)_{lk} (R^{\tilde{u}\dagger})_{li} + (R^{\tilde{u}})_{jk} (T_U^\dagger)_{lk} (R^{\tilde{u}\dagger})_{(l+3)i} \right] \right], \end{aligned} \quad (27)$$

where the sum over $k, l = 1, 2, 3$ is understood. The decay width for the process $\tilde{u}_i \rightarrow \tilde{u}_j h^0$ is given by

$$\Gamma(\tilde{u}_i \rightarrow \tilde{u}_j h^0) = \frac{1}{16\pi} \frac{\kappa(m_{\tilde{u}_i}^2, m_{\tilde{u}_j}^2, h^0)}{2m_{\tilde{u}_i}^3} |c_{\tilde{u}_i \tilde{u}_j h^0}|^2. \quad (28)$$

As usual, κ is defined by $\kappa^2(x, y, z) = (x - y - z)^2 - 4yz$.

B Experimental and theoretical constraints

Here we summarize the experimental and theoretical constraints taken into account in the present paper. The constraints on the MSSM parameters from the B-physics experiments and from the Higgs boson search at LHC are shown in Table 10.

The particle discovered most recently at LHC [27–29] is consistent with the SM Higgs boson. We identify this particle as the MSSM Higgs boson h^0 which is indeed SM-like in the decoupling Higgs scenarios considered in our paper. For the mass of the Higgs boson h^0 , we take an average of the central values of the ATLAS and CMS data [28, 29] and adding the theoretical uncertainty of $\sim \pm 2$ GeV [36] linearly to the experimental uncertainty at 2σ , we take $123 \text{ GeV} < m_{h^0} < 129 \text{ GeV}$.

In addition to these constraints we also require that our scenarios are consistent with the following experimental constraints:

(i) The LHC limits on the squark and gluino masses (at 95% CL) [48–51]: In the context of simplified models, gluino masses $m_{\tilde{g}} \lesssim 1 \text{ TeV}$ are excluded at 95% CL. The mass limit varies in the range 950–1125 GeV. First and second generation squark masses are excluded below 775 GeV. Bottom squarks are excluded below 600 GeV. In [51] a limit for the mass of the top-squark $m_{\tilde{t}} \gtrsim 500 \text{ GeV}$ for $m_{\tilde{t}} - m_{\text{LSP}} = 200 \text{ GeV}$ is quoted. Including mixing of \tilde{c}_R and \tilde{t}_R would even lower this limit [52].

(ii) The LHC limits on $m_{\tilde{\chi}_1^\pm}$ and $m_{\tilde{\chi}_1^0}$ from negative searches for charginos and neutralinos in leptonic final states [53].

(iii) The constraint on $(m_{A^0}, \tan\beta)$ from the MSSM Higgs boson searches at LHC [54].

(iv) The experimental limit on SUSY contributions on the electroweak ρ parameter [55]: $\Delta\rho(\text{SUSY}) < 0.0012$.

Furthermore, we impose the following theoretical constraints from the vacuum stability conditions for the trilinear coupling matrices [56]:

$$|T_{U\alpha\alpha}|^2 < 3 Y_{U\alpha}^2 (M_{Q\alpha\alpha}^2 + M_{U\alpha\alpha}^2 + m_2^2), \quad (29)$$

$$|T_{D\alpha\alpha}|^2 < 3 Y_{D\alpha}^2 (M_{Q\alpha\alpha}^2 + M_{D\alpha\alpha}^2 + m_1^2), \quad (30)$$

$$|T_{U\alpha\beta}|^2 < Y_{U\gamma}^2 (M_{Q\alpha\alpha}^2 + M_{U\beta\beta}^2 + m_2^2), \quad (31)$$

$$|T_{D\alpha\beta}|^2 < Y_{D\gamma}^2 (M_{Q\alpha\alpha}^2 + M_{D\beta\beta}^2 + m_1^2), \quad (32)$$

where $\alpha, \beta = 1, 2, 3$, $\alpha \neq \beta$; $\gamma = \text{Max}(\alpha, \beta)$ and $m_1^2 = (m_{H^\pm}^2 + m_Z^2 \sin^2 \theta_W) \sin^2 \beta - \frac{1}{2} m_Z^2$, $m_2^2 = (m_{H^\pm}^2 + m_Z^2 \sin^2 \theta_W) \cos^2 \beta - \frac{1}{2} m_Z^2$. The Yukawa couplings of the up-type and down-type quarks are $Y_{U\alpha} = \sqrt{2} m_{u_\alpha} / v_2 = \frac{g}{\sqrt{2}} \frac{m_{u_\alpha}}{m_W \sin \beta}$ ($u_\alpha = u, c, t$) and $Y_{D\alpha} = \sqrt{2} m_{d_\alpha} / v_1 = \frac{g}{\sqrt{2}} \frac{m_{d_\alpha}}{m_W \cos \beta}$ ($d_\alpha = d, s, b$), with m_{u_α} and m_{d_α} being the running quark masses at the weak scale and g being the SU(2) gauge coupling. All soft-SUSY-breaking parameters are given at $Q = 1 \text{ TeV}$. As SM parameters we take $m_W = 80.4 \text{ GeV}$, $m_Z = 91.2 \text{ GeV}$ and the on-shell top-quark mass $m_t = 173.3 \text{ GeV}$ [57]. We have found that our results shown are fairly insensitive to the precise value of m_t .

References

- [1] A. J. Buras *et al.*, Phys. Lett. B **500** (2001) 161 [arXiv:hep-ph/0007085].
- [2] G. D’Ambrosio, G. F. Giudice, G. Isidori and A. Strumia, Nucl. Phys. B **645** (2002) 155 [arXiv:hep-ph/0207036].
- [3] A. L. Kagan, G. Perez, T. Volansky and J. Zupan, Phys. Rev. D **80** (2009) 076002 [arXiv:0903.1794, hep-ph].
- [4] J. Beringer *et al.* [Particle Data Group Collaboration], Phys. Rev. D **86** (2012) 010001.
- [5] G. Hiller and Y. Nir, JHEP **0803** (2008) 046 [arXiv:0802.0916 [hep-ph]].
- [6] G. Hiller, J. S. Kim and H. Sedello, Phys. Rev. D **80** (2009) 115016 [arXiv:0910.2124 [hep-ph]].
- [7] M. Muhlleitner and E. Popenza, JHEP **1104** (2011) 095 [arXiv:1102.5712 [hep-ph]].
- [8] G. Bozzi, B. Fuks, B. Herrmann and M. Klasen, Nucl. Phys. B **787** (2007) 1 [arXiv:0704.1826 [hep-ph]].
- [9] B. Fuks, B. Herrmann and M. Klasen, Nucl. Phys. B **810** (2009) 266 [arXiv:0808.1104 [hep-ph]].
- [10] A. Bartl *et al.*, Phys. Lett. B **698** (2011) 380 [Erratum-ibid. B **700** (2011) 390] [arXiv:1007.5483 [hep-ph]].
- [11] M. Bruhnke, B. Herrmann and W. Porod, JHEP **1009** (2010) 006 [arXiv:1007.2100 [hep-ph]].
- [12] T. Hurth and W. Porod, JHEP **0908** (2009) 087 [arXiv:0904.4574, hep-ph].
- [13] A. Bartl *et al.*, Phys. Lett. B **679** (2009) 260 [arXiv:0905.0132 [hep-ph]].
- [14] A. Bartl *et al.*, Phys. Rev. D **84** (2011) 115026 [arXiv:1107.2775 [hep-ph]].
- [15] B. Fuks, B. Herrmann and M. Klasen, Phys. Rev. D **86** (2012) 015002 [arXiv:1112.4838 [hep-ph]].
- [16] Y. Nomura, M. Papucci and D. Stolarski, Phys. Rev. D **77** (2008) 075006 [arXiv:0712.2074 [hep-ph]].
- [17] A. Bartl, W. Majerotto and W. Porod, Z. Phys. C **64** (1994) 499 [Erratum-ibid. C **68** (1995) 518].
- [18] A. Bartl *et al.*, Phys. Lett. B **435** (1998) 118 [hep-ph/9804265].

- [19] A. Djouadi, J. L. Kneur and G. Moultaka, Nucl. Phys. B **569** (2000) 53 [hep-ph/9903218].
- [20] J. Cao, G. Eilam, K. -i. Hikasa and J. M. Yang, Phys. Rev. D **74** (2006) 031701 [hep-ph/0604163].
- [21] B. C. Allanach *et al.*, Comput. Phys. Commun. **180** (2009) 8 [arXiv:0801.0045 [hep-ph]].
- [22] F. Gabbiani, E. Gabrielli, A. Masiero and L. Silvestrini, Nucl. Phys. B **477** (1996) 321 [hep-ph/9604387].
- [23] J. A. Aguilar-Saavedra *et al.*, Eur. Phys. J. C **46** (2006) 43 [hep-ph/0511344].
- [24] W. Porod, Comput. Phys. Commun. **153** (2003) 275 [hep-ph/0301101].
- [25] W. Porod and F. Staub, Comput. Phys. Commun. **183** (2012) 2458 [arXiv:1104.1573 [hep-ph]].
- [26] F. Staub, T. Ohl, W. Porod and C. Speckner, Comput. Phys. Commun. **183** (2012) 2165 [arXiv:1109.5147 [hep-ph]].
- [27] CMS data: J. Incandela, plenary talk at 36th International Conference on High Energy Physics, Melbourne, Australia, 4-11 July 2012; ATLAS data: R. Hawking, plenary talk at 36th International Conference on High Energy Physics, Melbourne, Australia, 4-11 July 2012.
- [28] G. Aad *et al.* [ATLAS Collaboration], Phys. Lett. B **710** (2012) 49 [arXiv:1202.1408 [hep-ex]]; G. Aad *et al.* [ATLAS Collaboration], Phys. Lett. B **716** (2012) 1 [arXiv:1207.7214 [hep-ex]].
- [29] S. Chatrchyan *et al.* [CMS Collaboration], Phys. Lett. B **710** (2012) 26 [arXiv:1202.1488 [hep-ex]]; S. Chatrchyan *et al.* [CMS Collaboration], Phys. Lett. B **716** (2012) 30 [arXiv:1207.7235 [hep-ex]].
- [30] F. Brümmer, S. Kraml and S. Kulkarni, JHEP **1208** (2012) 089 [arXiv:1204.5977 [hep-ph]].
- [31] A. Arbey, M. Battaglia, A. Djouadi and F. Mahmoudi, JHEP **1209** (2012) 107 [arXiv:1207.1348 [hep-ph]].
- [32] R. Benbrik *et al.*, arXiv:1207.1096 [hep-ph].
- [33] W. Beenakker, R. Höpker, M. Spira, P. M. Zerwas, JHEP **08** (2010), 098 [arXiv:1006.4771 [hep-ph]].
- [34] T. Hahn, Comput. Phys. Commun. **140** (2001), 418 [arXiv:hep-ph/0012260].

- [35] T. Hahn and C. Schappacher, *Comput. Phys. Commun.* **143** (2002), 54 [arXiv:hep-ph/0105349].
- [36] S. Heinemeyer, O. Stal and G. Weiglein, *Phys. Lett. B* **710** (2012) 201 [arXiv:1112.3026 [hep-ph]].
- [37] W. -S. Hou, *Phys. Rev. D* **48** (1993) 2342.
- [38] S. Vecchi, parallel talk at 36th International Conference on High Energy Physics, Melbourne, Australia, 4-11 July 2012.
- [39] M. S. Carena *et al.*, *Phys. Rev. D* **74** (2006) 015009 [hep-ph/0603106]; see also P. Ball and R. Fleischer, *Eur. Phys. J. C* **48** (2006) 413 [hep-ph/0604249].
- [40] S. Stone, plenary talk at 36th International Conference on High Energy Physics, Melbourne, Australia, 4-11 July 2012.
- [41] M. Misiak *et al.*, *Phys. Rev. Lett.* **98** (2007) 022002 [hep-ph/0609232].
- [42] M. Iwasaki *et al.* [Belle Collaboration], *Phys. Rev. D* **72** (2005) 092005 [hep-ex/0503044]; B. Aubert *et al.* [BABAR Collaboration], *Phys. Rev. Lett.* **93** (2004) 081802 [hep-ex/0404006].
- [43] T. Huber, T. Hurth and E. Lunghi, *Nucl. Phys. B* **802** (2008) 40 [arXiv:0712.3009 [hep-ph]].
- [44] M. Perrin-Terrin, parallel talk at 36th International Conference on High Energy Physics, Melbourne, Australia, 4-11 July 2012.
- [45] J. Albrecht, plenary talk at Hadron Collider Physics Symposium 2012 (HCP2012), Nov 12-16, 2012, Kyoto, Japan.
- [46] R. Barbieri, summary talk at 36th International Conference on High Energy Physics, Melbourne, Australia, 4-11 July 2012.
- [47] K. Trabelsi, plenary talk at ICHEP2010, PoS (ICHEP 2010) 566.
- [48] A. Parker, plenary talk at 36th International Conference on High Energy Physics, Melbourne, Australia, 4-11 July 2012; M. Backes, parallel talk at the same conference.
- [49] G. Aad *et al.* [ATLAS Collaboration], arXiv:1208.0949 [hep-ex]; G. Aad *et al.* [ATLAS Collaboration], arXiv:1208.4688 [hep-ex]; G. Aad *et al.* [ATLAS Collaboration], ATLAS-CONF-2012-103; G. Aad *et al.* [ATLAS Collaboration], arXiv:1206.1760 [hep-ex]; S. Chatrchyan *et al.* [CMS Collaboration], <http://cdsweb.cern.ch/record/1460434>; S. Chatrchyan *et al.* [CMS Collaboration], <http://cdsweb.cern.ch/record/1460433>; S. Chatrchyan *et al.* [CMS Collaboration], arXiv:1208.4859 [hep-ex]; S. Chatrchyan *et al.* [CMS Collaboration], arXiv:1205.6615 [hep-ex]; S. Chatrchyan *et al.* [CMS Collaboration], arXiv:1204.3774 [hep-ex].

- [50] A. Cakir [CMS Collaboration], arXiv:1211.6289 [hep-ex]; G. Aad *et al.* [ATLAS Collaboration], arXiv:1209.2102 [hep-ex]; G. Aad *et al.* [ATLAS Collaboration], arXiv:1208.4305 [hep-ex]; G. Aad *et al.* [ATLAS Collaboration], arXiv:1208.2590 [hep-ex]; G. Aad *et al.* [ATLAS Collaboration], arXiv:1208.1447 [hep-ex]; G. Aad *et al.* [ATLAS Collaboration], arXiv:1207.4686 [hep-ex]; G. Aad *et al.* [ATLAS Collaboration], arXiv:1203.6193 [hep-ex]; G. Aad *et al.* [ATLAS Collaboration], arXiv:1203.5763 [hep-ex]; G. Aad *et al.* [ATLAS Collaboration], Phys. Rev. Lett. **108** (2012) 181802 [arXiv:1112.3832 [hep-ex]].
- [51] S. Chatrchyan *et al.* [CMS Collaboration], arXiv:1301.2175 [hep-ex]; S. Chatrchyan *et al.* [CMS Collaboration], arXiv:1303.2985 [hep-ex].
- [52] M. Blanke, G. F. Giudice, P. Paradisi, G. Perez and J. Zupan, arXiv:1302.7232 [hep-ph].
- [53] G. Aad *et al.* [ATLAS Collaboration], arXiv:1208.3144 [hep-ex]; S. Chatrchyan *et al.* [CMS Collaboration], [arXiv:1209.6620 [hep-ex]].
- [54] S. Chatrchyan *et al.* [CMS Collaboration], Phys. Lett. B **713** (2012) 68 [arXiv:1202.4083 [hep-ex]].
- [55] G. Altarelli, R. Barbieri and F. Caravaglios, Int. J. Mod. Phys. A **13** (1998) 1031 [hep-ph/9712368].
- [56] J. A. Casas and S. Dimopoulos, Phys. Lett. B **387** (1996) 107 [hep-ph/9606237].
- [57] E. Shabalina, plenary talk at ICHEP2010, PoS (ICHEP 2010) 561.